Publication and copyright notes

Title:

Influence of Surface Design on the Solid Lubricity of Carbon Nanotubes-Coated Steel Surfaces

Authors:

C. Schäfer, L. Reinert, T. MacLucas, P. Grützmacher, R. Merz, F. Mücklich, S. Suarez

This is a post-peer-review, pre-copyedit version of an article published in *Tribology Letters*

The final authenticated version is available online at: https://doi.org/10.1007/s11249-018-1044-8

Cite as:

Schäfer, C., Reinert, L., MacLucas, T. et al. Tribol Lett (2018) 66: 89. https://doi.org/10.1007/s11249-018-1044-8

Influence of surface design on the solid lubricity of carbon nanotubes coated steel surfaces.

C. Schäfer [1], L. Reinert [1], T. Maclucas [1], P. Grützmacher [1], R. Merz [2], F. Mücklich [1] and S. Suarez [1].

[1] Department of Materials Science, Saarland University, Campus D 3.3, 66123 Saarbrücken, Germany

[2] Institut für Oberflächen- und Schichtanalytik GmbH, Trippstadter Straße 120, 67663 Kaiserlautern, Germany

Abstract

Topographically designed surfaces are able to store solid lubricants, preventing their removal out of the tribological contact and thus significantly prolonging the lubrication lifetime of a surface. The present study provides a systematic evaluation of the influence of surface structure design on the solid lubrication effect of multi-walled carbon nanotubes (MWCNT) coated steel surfaces. For this purpose, direct laser writing using a femtosecond pulsed laser system is deployed to create surface structures, which are subsequently coated with MWCNT by electrophoretic deposition. The structural depth or aspect ratio of the structures and thus the lubricant storage volume of the solid lubricant is varied. The frictional behavior of the surfaces is recorded using a ball-on-disc tribometer and the surfaces are thoroughly characterized by complementary characterization techniques. Efficient lubrication is achieved for all MWCNT coated surfaces. However, and in contrast to what would be expected, it is shown that deeper structures with larger lubricant storage volume do not lead to an extended lubrication lifetime and behave almost equally to the coated unstructured surfaces. This can be attributed, among other things, to differences in the final surface roughness of the structures and the slope steepness of the structures, which prevent efficient lubricant supply into the contact.

Keywords

Solid lubrication; Laser structuring; Carbon nanotubes; Coating

1. Introduction

In the past years, it has been extensively reported, that precisely produced periodic surface structures positively influence friction and wear in mechanically loaded components for example by reducing the real contact area and trapping wear debris [1–3]. To create those surface structures, there is a great number of possible techniques available, such as micro coining [4], burnishing [5], lithography and anisotropic etching [6], honing [7] and laser surface texturing (LST) [1]. Regarding LST, a distinction can be made between direct laser writing (DLW) and direct laser interference patterning (DLIP). While DLIP is based on the interference of several laser beams, making high speed surface patterning possible [8,9], DLW provides a greater flexibility of the created structures (e.g. higher aspect ratios) through successive surface processing.

Well defined depressions on a textured surface may also act as a reservoir for liquid and solid lubricants and are therefore able to continuously provide the loaded contact area with lubricant, resulting in a reduction of friction and wear and thus prolonging the duty life of the tribological stressed components [10–13].

Concerning solid lubricants, materials like graphite [14], MoS_2 [13,14], WS_2 [15] and carbon nanotubes (CNTs) [16] turned out to be very effective in lowering the coefficient of friction (COF). Among those, particularly CNTs are exceedingly promising candidates due to their unique properties, such as their sp^2-hybridization state and the resulting binding conditions, their unique form, their high aspect ratio as well as their high flexibility. Numerous studies have shown, that CNTs can significantly contribute to reduce friction and wear in tribological applications, for example as a reinforcing second phase in composites [17–22], as a solid protective film [23–27] or as an additive in liquid lubricants [28–31]. Scharf et al. [19] were able to trace the self-lubricating properties of Ni/CNT-composites to the formation of a lubricating film of graphitic nature, which protects the contacted surface against tribo-chemical reactions (e. g. oxidation) and leads to a low shear strength within the contact area. Furthermore, the lubricating effect of CNTs is often linked to their ability to roll and slide over surfaces [32] and to act as spacers between a contacting tribological pair [33]. Dickrell et al. [26,34] pointed out differences in the tribological behavior of CNT films depending on their orientation on the substrate surface. The horizontally aligned nanotubes showed an immense lowering of

COF in comparison to the vertically arranged CNTs due to their ability – in case of the horizontal alignment – to perform complex motions that combine sliding and rolling [32].

Regarding the manufacturing of CNT coatings, there is a large variety of possible techniques, e. g. spray coating [35], dip coating [36], drop casting [22,37], chemical vapor deposition (CVD) [38] or electrophoretic deposition (EPD) [39–41]. Out of those, EPD offers a variety of benefits, such as low costs, simple procedure, reproducibility, good control of the layer thickness, microstructural homogeneity of the coatings as well as the possibility to deposit on complex shapes [42–44].

Despite the above-mentioned advantages, both, laser-induced surface structures as well as coatings containing solid lubricants involve drawbacks related to friction and wear. Periodical structures may be gradually removed and solid lubricants may be transported out of the contact area by continuous removal, severely hindering their positive tribological effects [2,3,22]. However, a combination of both methods could lead to an overcoming of those drawbacks.

Recently, Reinert et al. [45] investigated the tribological behavior of DLIP-structured and CNT-coated steel substrates. They could show, that the combination of both techniques facilitates the storage of CNTs within the depressions of the periodic surface structure, whereby the CNTs are continuously fed into the contact area thus reducing friction and wear to a significant degree. Compared to the isolated used methods, the period, in which a noticeably reduced COF is present, can be prolonged many times. The line-like structures complete their task as reservoirs for solid lubricant until they are completely removed.

The results shown in [45] form the basis for the motivation of this study. The increase in aspect ratio of the structures by producing deeper structures and thus increasing the volume of the reservoirs, could lead to a further improvement of the tribological system. However, with the nanosecond laser system used in [45], the achievable structural depths are limited to approximately 1 µm [11,46]. With an ultra-short pulsed laser system, material is removed by ablation, preventing the formation of piled up, molten and re-solidified material, thus leading to surfaces with a higher load-bearing capacity and a larger lubricant storage reservoir at the same time [47,48]. For the given reasons, this study investigates the influence of the lubrication reservoir volume on the tribological behavior of CNT-coated steel samples. For varying the structure depth, an ultra-short pulsed laser system with a pulse duration of 100 fs and a

repetition rate of 1 kHz is used. Due to the above-mentioned advantages over the other techniques, EPD is used for producing the CNT-coatings.

2. Materials and methods

2.1 Materials

MWCNTs synthesized by catalytic chemical vapor deposition (CCVD) were purchased from Graphene Supermarket (USA). Their diameter distribution ranged between 50-85 nm and their length between 10-15 μm. The as-received carbon content is over 94%. The substrates consisted of stainless steel plates (AISI 304 grade) with a thickness of 1 mm and a (20x20) mm^2 area. The surface is finished to a mirror polishing (R_a = 16.3 ± 5.2 nm). Before structuring the platelets, the surfaces were cleaned rigorously to remove possible contaminants. The cleaning process consisted of three consecutive 10 min ultrasound baths (Bandelin Sonorex RK514BH) in cyclohexane, acetone and isopropanol alternated with deionized water rinsing followed by drying with pressurized air.

2.2 Characterization techniques

The steel surfaces were topographically characterized by confocal laser scanning microscopy (LEXT OLS4100, Olympus) with a laser wavelength of 405 nm. The lateral and vertical resolution of the equipment is 120 and 10 nm, respectively. The measurements were carried out with a 50X objective (N.A. = 0.95).

The coatings and wear tracks were morphologically characterized with a field emission scanning electron microscopy/ focused ion beam (FE-SEM/FIB) Helios NanoLab 600 dual beam workstation (FEI) equipped with an EDS detector (EDAX).

The structural characteristics of the CNTs and the oxide development were observed by Raman spectroscopy on an inVia Raman microscope (Renishaw). The used laser wavelength was 532 nm. The laser power on the sample was 2 mW (50X objective, N. A. 0.9), resulting in a spot size of 5 μm. The spectral resolution is 1.2 cm^{-1}. All the acquired spectra are further post-processed by removing the experimental background and fitting the characteristic peaks with Lorentz functions [49].

Oxide layer thickness and chemistry were characterized by AES (Auger electron spectroscopy) on different areas of the micro structured steel platelets after laser irradiation. The analysis was done by sputter depth profiles. Here the 10keV, 10nA primary electron beam is scanned selectively over micro regions, defined before in SEM micrographs, alternatingly followed by single sputter steps with a Ar+ beam (beam energy 2keV) scanned over 2mm x 2mm. With the same ion gun adjustments the oxide layer of a standard reference sample (60nm Ta2O5 oxide layer on Ta) was sputtered through in 490 min.

2.3 Ultra-short pulsed laser surface structuring

The surfaces of the steel platelets are structured by direct laser writing (DLW) using a femtosecond pulsed laser system (Spectra-Physics, Ti:Sapphire laser) with a pulse length of 100 fs, a wavelength of 800 nm and a pulsing frequency of 1 kHz. The laser is focused on the sample surface with an output power of 30 mW producing a spot size of 10 - 15 µm Line-like structures are created on the steel platelets by moving them with a two axis motorized stage in a meander-like pattern. Subsequently, the sample is rotated by 90° and the process is repeated, finally resulting in a cross-like structure. Cross-like structures are chosen instead of line-like structures as the tribological measurement is performed in a rotational mode. Thus, a line-like structure would behave highly anisotropic. According to the pulse frequency, the stage velocity is adapted so that the individual laser pulses overlap by 50 % and an almost constant structural depth of 1 µm is obtained for one laser pass. In order to create a structure depth of 3 µm, the laser beam is moved four times in total over each line. The distance from line to line is chosen to be 50 µm.

2.4 Coating production by electrophoretic deposition

Prior to the deposition, the CNTs were acid-functionalized following the procedure described in a previous paper by [50]. Subsequently, the functionalized CNTs (9 mg) were dispersed in ethanol (90 mL) with triethylamine (13 mL) as an additive. The function of the additive is to improve the deposition rate of the dispersed CNTs by increasing the degree of deprotonation of the carboxy groups on the particles' surface. During the first part of the dispersion process, the colloidal solution is homogenized in a shear mixer (Ultra-Turrax T25, IKA-Germany) at 8000 rpm for 5 minutes. Secondly, the solution is further dispersed in an ultrasonic bath (Bandelin Sonorex RK514BH) for 20 min. The deposition occurred at a voltage of 40 V over a period of 10 min on the anode. During deposition, the electrodes are arranged in parallel to

ensure the formation of a uniform electric field between the electrodes and therefore a homogeneous coating. The separation of the electrodes remained constant at 1.3 cm. After the deposition, the coated substrate was immersed in ethanol in order to wash out the additive.

2.5 Tribological experiments

The tribological characterization was performed using a ball-on-disk micro-tribometer (CSM Instruments) working in rotational mode. The tribometer is placed within an environmental chamber to control temperature and humidity during the experiments. The chosen track radius was 5 mm and the normal load was 1 N. The linear velocity was set to 1 cm/s so as to allow the lubricant to be pressed into the surface depressions and not to be swept away from the surface. The friction force was measured by a linear variable differential transformer (LVDT). During the experiments, the temperature and humidity were kept constant at 25 °C and 45 %, respectively. The selected static counterpart was an Al_2O_3 ball (Anton Paar GmbH), with a 6 mm diameter and a surface roughness of R_a: 23.8 ± 1.8 nm. As the alumina ball is much harder than the steel surface, wear is expected to occur mainly on the steel surface.

3. Results and discussion

3.1 Initial state characterization

The fabricated surfaces and the corresponding cross-sections are depicted using laser-scanning microscopy in **Fig. 1**.

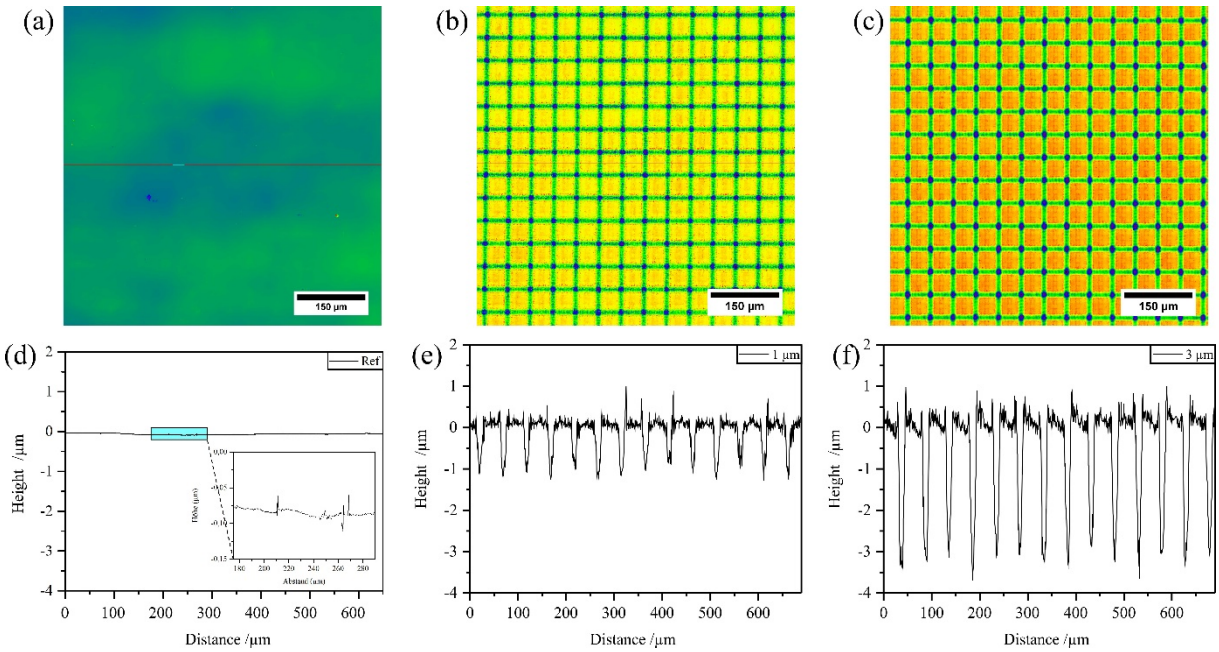

Figure 1 – Height profile color maps of (a) polished steel plate, (b) 1 µm DLW structure and (c) 3 µm DLW structure. (d-f) profile of the surfaces measured at the corresponding red lines of the color maps.

The surfaces show a homogeneous surface structure with a reproducible structural depth of 1 µm or 3 µm, respectively. Particularly for the structural depth of 3 µm (**Fig. 1 c and f**), the formation of high profile deposits is observed at the edges of the surface depressions. These can be traced back to a displacement of the molten from the ablation zone as well as to a re-depositioning of ablated material [51]. The effect is also present for the structures with a depth of 1 µm, but to a much lesser degree, as can be seen in **Fig. 1 b and e**. Furthermore, it has to be mentioned, that the crossing points of the laser structures present surfaces depressions, which are twice as deep. This is a consequence of being exposed to the laser beam in case of the horizontal and vertical structuring process. In order to evaluate the load bearing capacity of the surfaces, Abbott-Firestone curves [52] are plotted in **Fig. 2** for the reference as well as for the laser structured surfaces.

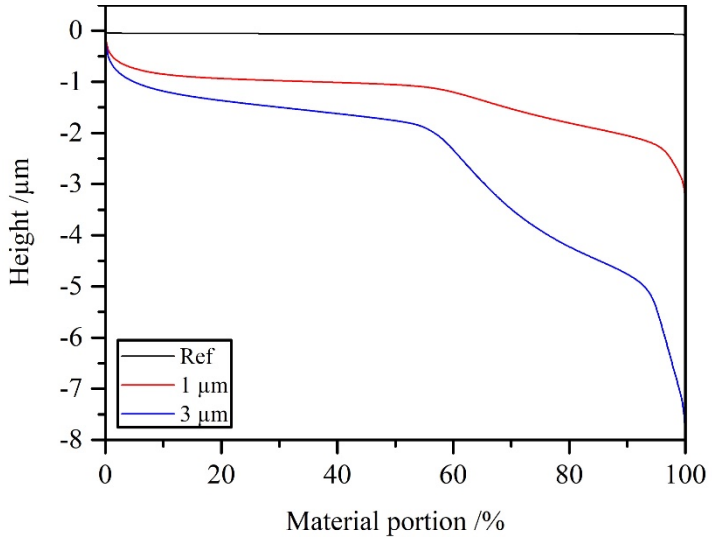

Figure 2 – Abbott-Firestone curves of the reference surface and the laser-structured surfaces with a depth of 1 µm and 3 µm, respectively.

It is observed that the high profile deposits represent the first 5 % of the material portion for the structured samples. However, in case of the 3 µm-curve, the slope within this section is much higher than for the 1 µm-curve, indicating the presence of a large amount of rather pointy asperities due to displacement of molten material and material re-depositioning at the edges of the surface depressions. For a material portion between 5 % and 55 %, the 1 µm-curve is almost in parallel to the reference curve, thus presenting a smooth surface with a high load bearing capacity.

This is traced back to the almost unmodified large surface plateaus of 35 x 35 μm^2 in size. The 3 µm-curve drops twice as much in this section, which speaks for a surface with a higher roughness on the above-mentioned surface plateaus, possibly being a consequence of material re-depositioning and the generation of laser induced periodic surface structures (LIPSS) [53]. The latter result from the interference between the incident and the already reflected laser beam. For strongly absorbing materials, like metals and semiconductors, low-spatial-frequency-LIPSS (LSFL) with periodicities in the range of the used laser wavelength and an orientation perpendicular to the polarization of the laser beam can be observed.. The next section (55 % - 95 %) is based on the generated surface depressions, which show a decrease in height of 1 µm or 3 µm, respectively. The last part of the curve (95 % - 100%) corresponds to the intersecting points during the laser structuring process, consequently being twice as deep.

Subsequently, the surfaces were chemically characterized using Auger electron spectroscopy. For this purpose, the laser structured surface (depth of 3 µm) and the unstructured steel reference is measured. The results can be found in **Fig. 3**.

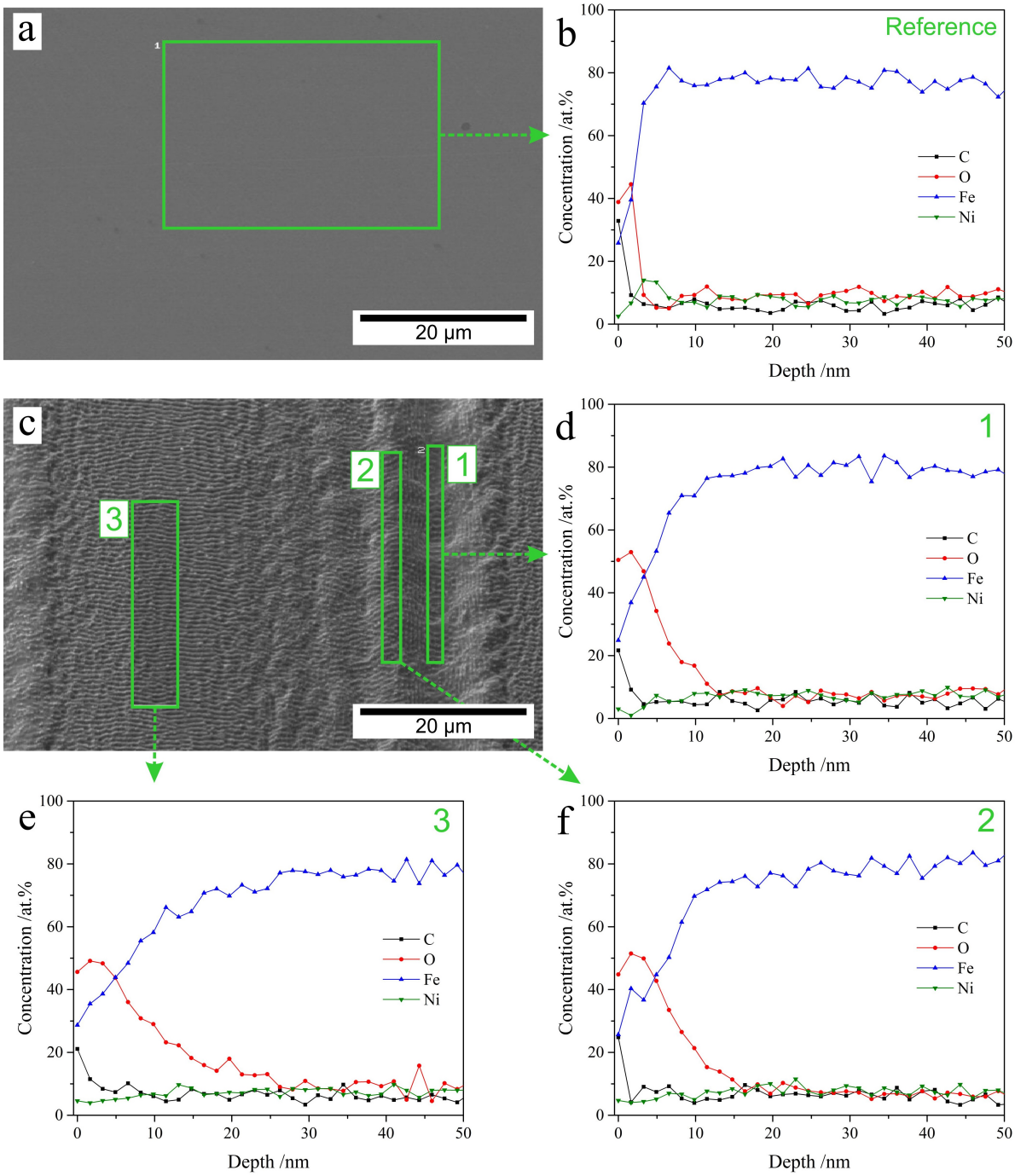

Figure 3 – SEM micrographs of a) the unstructured steel reference and c) the laser structured surface with a structural depth of 3 µm. The marked regions 1-3 in c) are measured by AES in d), e) and f), respectively. The corresponding AES characterization is also performed for the unstructured reference in b).

In the case of the laser structured surface, three areas are distinguished (1-3), with 1 representing the ablation area, 2 the edge of the surface depression where high profile deposits are found and 3 the area that was not subjected to ablation. By comparing the graph of the unstructured reference with the graphs of the structured surface, it is obvious, that the concentration in oxygen is increased for the laser-structured surface. This could be explained with the ablated metal being highly reactive, and thus being oxidized during this process. Due to the re-deposition of ablated metal in area 2 and 3, the areas are fully covered with metal oxides [54]. A quantitative comparison of oxidation between the different areas is not possible, since the areas provide different surface roughness. Thus, with the surfaces being measured after different sputtering times, oxides that were present between surface roughness asperities are possibly not removed and contribute to the AES signal even for higher depths. However, it can be concluded that light surface oxidation of the structured surfaces must be taken into account when discussing the tribological results. In addition, the above-mentioned LIPSS can be observed all over the sample.

Finally, the surfaces were coated with MWCNT using EPD. **Fig. 4** shows the obtained coated surfaces.

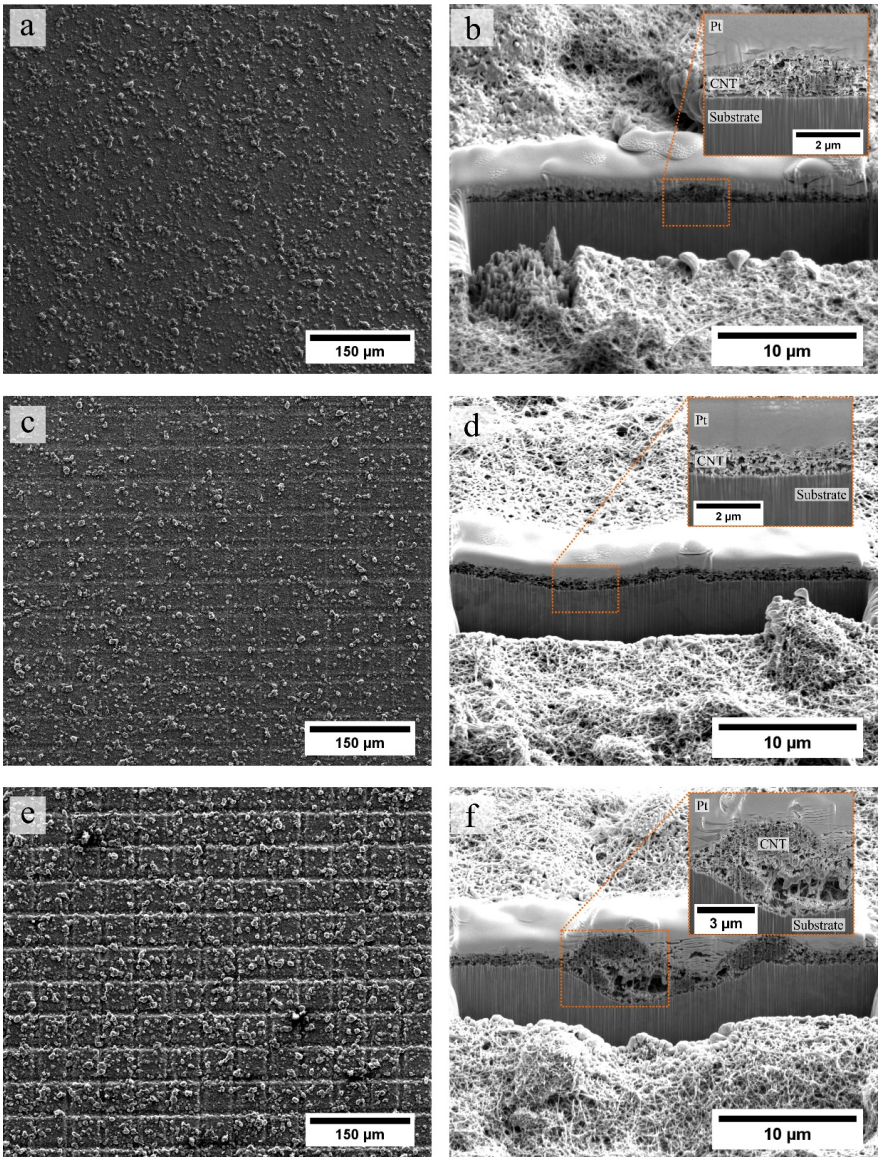

Figure 4 – Electron micrographs of the resulting EPD coatings for (a) coated reference, (c) 1 µm deep structure and (e) 3 µm deep structure. The images (b, d and f) show SEM/FIB cross sections of the corresponding coatings. The insets show a detailed view of the interfaces between the coating and the substrate for each case.

In all cases, CNT agglomerates are still observed on the surfaces. Furthermore, no evident uncovered areas or cracks in the coatings are identified. The SEM/FIB cross sections show a homogeneous thickness of approximately 1 µm in all cases. It is worth noting that in the 3 µm depth sample (**Fig. 4f**), some cavities in the coating at the topographical minimum are detect-

ed. All samples display a seamless interface between coating and substrate (insets of **Fig. 4 b, d** and **f**).

3.2 Frictional behavior

The temporal evolution of the coefficient of friction is shown in **Fig. 5**. In the short-term tests (a), the COF of the uncoated samples (both, unstructured and structured) increases within the first 1000 cycles, finally reaching a steady state COF close to 0.9. This value is quite high for this tribological pair and could be related to a continuous growth of an oxide layer. Thus the initially present higher surface oxidation of the laser-textured surfaces seems to play a minor role for the running in process of the uncoated surfaces. When observing the behavior of the coated samples, the difference in friction is quite significant. The unstructured, coated sample shows a significantly lower COF than the uncoated samples with an irregular evolution of the COF. This instability is related to the re-accommodation of solid lubricant with each rotating cycle, in which the CNTs are driven inhomogeneously towards the direct contact area. However, their lubrication capacity is still active during these cycles. Regarding the CNT-coated laser structures, both show a stable COF throughout the first 2000 cycles, with values around 0.2. Again, the stability in this case is related to how the CNTs are brought into contact during the test. This proves the reservoir-effect generated by the depressions storing and sequentially releasing lubricant.

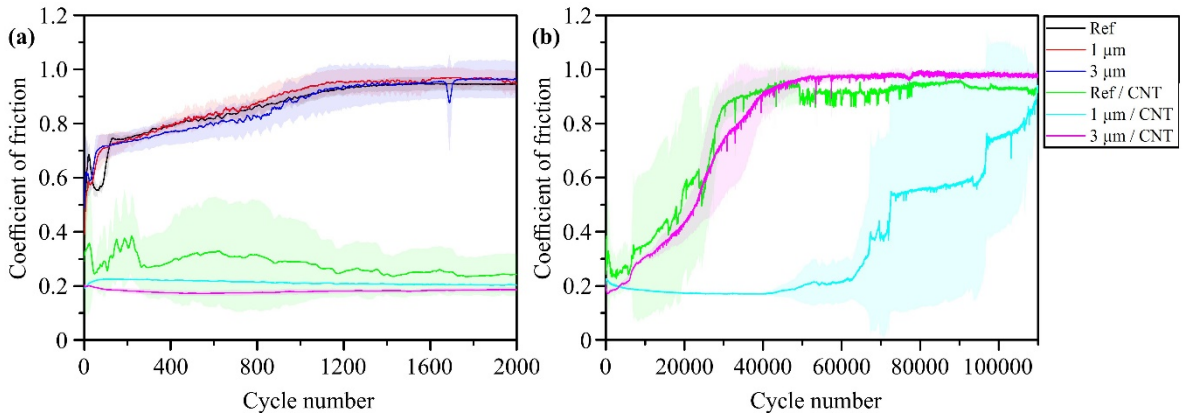

Figure 5 – (a) Short-term evolution of the coefficient of friction for the uncoated and coated samples. (b) Long-term development of the coefficient of friction for the coated samples.

If the focus is then placed on the long-term behavior of the surfaces, the analysis for the uncoated samples becomes inconsequential, since they have already reached their steady state at

lower cycles. Hence, the long-term analysis only refers to the CNT-containing systems, which is shown in **Fig. 5b**.

After an initial slight drop, the Ref/CNT sample shows a continuous increase in COF until reaching steady state after approximately 45000 cycles. It is noticeable that the COF standard deviation of this sample, which is already pronounced at the beginning, increases considerably from approx. 7000 cycles. This can be justified by the fact that individual measurements show an early or late sharp increase in COF and ultimately reach reference conditions earlier or later than the mean value. All individual measurements show this rapid increase between 7000 and almost 26000 cycles. Furthermore, it can be observed that the curve shows several drops during the ascent, which might be correlated to fluctuations in concentration of CNT within the direct tribological contact area.

In the case of the structured and coated samples, both present an unexpected and counterintuitive development of the COF. The COF value of 3µm/CNT surpasses that of 1µm/CNT after about 3400 cycles. Contrary to the sample Ref/CNT, there are no leaps during the rise of the COF. The COF of the 3 µm/CNT sample continuously grows until the reference steady state COF value is reached at approx. 50000 cycles, similar to the Ref/CNT sample. In contrast, the curve of 1µm/CNT excels by a stable curve with a low COF and very low standard deviation. The standard deviation becomes significant only after about 40000 cycles. Possible causes for this could be a degradation of the CNTs or their removal from tribological contact [45].

The considerably earlier increase in the COF of the sample 3µm/CNT can be related to several causes. On one hand, the surface structures, characterized in **Fig. 1** and **4,** show a steeper profile of the structural flanks with increasing depth (17 ± 3 ° and 22 ± 2 ° for 1 µm and 3 µm, respectively). As the lubrication mechanisms of the CNT coated laser structures was described to be based on compression and elastic restoration of the CNTs in the depressions in Reinert et al. [45], this effect might not be as pronounced for the 3 µm deep structures. Steeper profile flanks and also cavities within the CNT coating (see **Fig. 4 f**) are associated with a reduced elastic restoration effect, compared to the 1 µm deep structure thus making it more difficult to draw the CNTs from the structural cavities into tribological contact [45]. This means that the lubrication effect is lost at an early stage despite still having filled lubricant reservoirs available. Furthermore, the structures of this sample type are not completely filled to the level of the supporting surface with CNTs (see **Fig. 4 e-f**). During the first cycle of the

Al_2O_3 counterpart, the CNTs are pressed into the cavities and thus the initial cavities are reduced. This further prevents the elastic restoration of CNTs after the alumina ball has passed. As a result, CNTs cannot further be removed from the depressions by adhesion to the ball during the following cycle of the counterpart. For this reason, the CNTs gradually disappear from the contact zone and direct contact between the substrate and counterpart occurs, causing the COF to rise and tend to the reference value. In addition, the larger number and height of oxidized material pilings at the edges of the cavities can also play a pivotal role. The high profile deposits (as observed in **Figure 1 e-f**) could be plastically deformed during the first passes, consequently leading to a partial hindering of a further lubricant supply. This effect could be fortified by premature abrasion of these asperities and the associated generation of oxidic wear particles, which could be stored on top of the CNTs in the depressions, hindering an efficient lubricant supply and additionally increasing the abrasive component of the tribological system.

Fig. 5b further shows that the sample type 1µm/CNT does not reach the steady state value of the reference sample (on average) until 110000 cycles have been completed. The stepwise increments in the averaged COF curve and the large standard deviation result from the different points in time at which the tested samples experience a sudden increase from a very low COF to the reference steady state COF value. Possible causes for this observation are similar to the two other coated sample types (Ref/CNT and 3µm/CNT), a degradation of the CNTs as well as the removal of the CNTs from the tribological contact. Due to wear, the laser-generated surface structures are completely removed after a certain time, so that there are no more lubricant reservoirs that could supply the contact with CNTs. All coated substrates show a similar lubricating effect as that reported in [45]. During tribological stress, the CNTs have large areas available on which they can roll/slide between the substrate and counterbody and thus reduce the COF before they are pressed into the nearest structural depression. When compared to the uncoated reference state, a significant COF reduction for the Ref/CNT is observed (factor of 4.5). With the degree of frictional reduction for the structured samples being even more pronounced (factor of 6), the lubrication lifetime of the 1µm/CNT sample is prolonged (factor of 9).

3.3 Wear track and tribo-chemical analysis

In order to investigate the underlying lubrication mechanism, the structural state of the CNTs has to be examined. For this purpose, Raman spectroscopy analysis of the CNTs at both, the inside and outside of the wear tracks, is performed and compared to the spectra which were obtained by measuring pure CNT powder before the EPD coating process (black curve in the following figures). Despite the structural integrity analysis of the particles, also a tribo-chemical characterization is performed, focusing on the presence of oxides in the wear tracks. Raman analysis of the wear tracks was performed for all coated samples after 18000 cycles and after reaching the reference steady state friction coefficient (end of lubrication lifetime). In this way, failure mechanisms can be accurately evaluated.

3.3.1. Ref/CNT sample

For the sample type **Ref/CNT after 18000 cycles**, the typical Raman bands of CNTs are observed in all measurement points (**Fig. 6a**). The measurements of the pure CNT powder (**Fig. 6a, Ref spectrum**) confirm the typical literature values for the D, G and G' bands [55,56]. The D-peak of the studied MWCNTs is placed at a wavenumber of 1350.4 cm^{-1}, the G-peak at 1582.1 cm^{-1} and the G'-peak at 2696.1 cm^{-1}. Furthermore, two additional peaks with low intensities can be identified immediately before and after the G' peak. The peak at 2450 cm^{-1} corresponds to a non-dispersive phonon mode [57] and that at a wavenumber of approx. 2900 cm^{-1} is due to a harmonic of the LO mode [58]. However, since these two resonances do not provide quantifiable information on the structural condition of the CNTs, they are neglected in the following for the interpretation of the tribochemistry. In contrast to that, the intensity ratio of the D- and the G-band (I_D/I_G) can be correlated to the defect index and thus, the crystalline domain size [56].

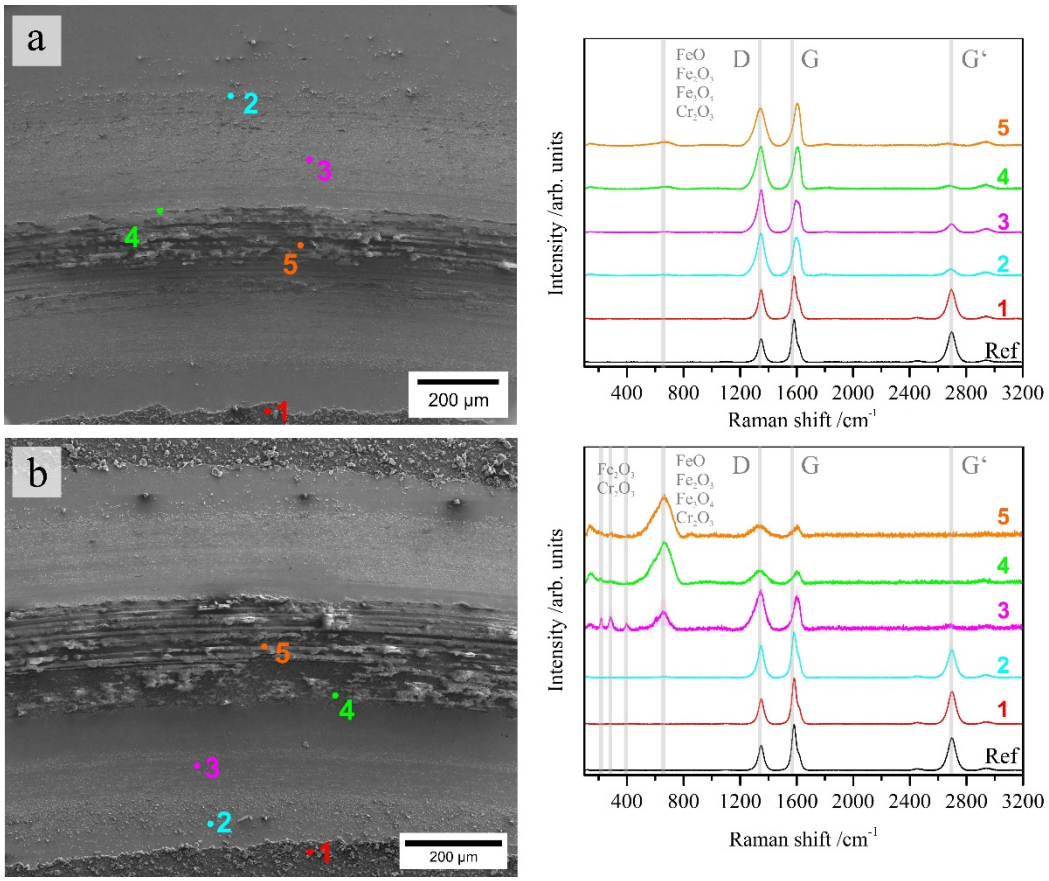

Figure 6 – Electron micrograph of a section of the wear track and Raman spectra acquired at specific sites after (a) 18000 cycles and (b) after reaching the reference steady state friction coefficient (24400 cycles).

Interestingly, even at the center of the wear track (position of maximum contact pressure) CNTs with moderate I_D/I_G values are detected and only weak oxide peaks are recorded at 660 cm^{-1} (convolution of FeO, Fe_3O_4 and Fe_2O_3 vibrational modes) [59–61]. However, from position 2 inwards, the G-band is already shifted noticeably to higher wavenumbers (approx. 1600 cm^{-1}), as can be seen in **Table 1**. The aforementioned shift of the G-band was part of past investigations by Ferrari and Robertson [49], which subdivide the structural changes of graphitic materials into a phenomenological three-stage model. Depending on the position of the G-peak (X_{CG}) and based on the defect index (I_D/I_G), the model describes the transition from a graphitic structure via nanocrystalline graphite to disordered carbon (mainly sp^3-hybridized). Since CNTs at their initial state are basically a highly crystalline graphitic modification, this model is suitable to track the structural integrity of the MWCNTs.

With the G-band upshifting and the increased defect index of over 1 (CNT reference: 0.55), a structural transition of the CNTs towards nanocrystalline graphite is established. The sharp increase in COF from 14700 cycles onwards (0.71 after 18000 cycles) is likely due to the failure of lubrication by the CNTs. With lubrication failing but nanocrystalline graphite being still present in the wear track, the lubrication mechanism of CNT seems not to be based on a pure graphite type lubrication - the shearing-off of individual graphene layers - but can be attributed also to an efficient separation of the surfaces and complex motions (sliding/rolling) of the CNTs. The degradation of the CNTs and thus lubrication failure is strongly related to the contact pressure gradient towards the center of the track. Consequently, a tribologically-induced oxide layer is formed with Raman peaks being observed at 225 cm^{-1} (α -Fe_2O_3 band), at 270 cm^{-1} (convolution of α -Fe_2O_3 and Cr_2O_3), at 380 cm^{-1} ((Fe, Cr)O_3 band) and finally at 660 cm^{-1} [59–61]. The oxide formation results from local heating derived from high contact pressures. This layer can be further disrupted, forming oxidic abrasive third bodies.

Table 1 – Structural assessment of the CNTs at different stages of the tribological test.

After 18000 cycles					**After reaching steady state reference COF**				
Sample		**I_D/I_G**	**X_{CG}**		**Sample**		**I_D/I_G**	**X_{CG}**	
	Ref	0.55	1582.1			Ref	0.55	1582.1	
Ref/CNT	1	0.70	1583.1		Ref/CNT (24.4k cycles)	1	0.56	1582.1	
	2	1.12	1599.4			2	0.71	1582.1	
	3	1.32	1594.0			3	1.18	1600.6	
	4	1.02	1603.8			4	1.06	1598.4	
	5	0.89	1603.8			5	1.03	1600.6	

Fig. 6b shows a wear track overview and the Raman spectra of the characteristic points in and around the wear track of the sample **Ref/CNT** after reaching steady state reference COF at 24400 cycles. The general statement of this evaluation is similar to the analysis of the wear track after 18 000 cycles. However, the Raman spectra acquired in the interior region (measurement points 3 to 5) present even more significant changes. First, the formation of oxides is increasing towards the center of the wear track. In agreement with this observation, a steady decrease in the intensity of the CNT peaks and the increasing values of the defect index (I_D/I_G) show a further cumulative degradation of the CNTs towards the center of the wear track compared to the situation after 18000 cycles. Moreover, the G'-band vanishes from the outer edge of the central wear track (position 4). In addition, a noticeable shift in the G-peak position up to a wavenumber of approx. 1600 cm^{-1} can be observed (**Table 1)**.

It is thus evident that the CNTs are no longer (in sufficient quantity) in tribological contact, which means that they can no longer fulfill their function as spacers between the substrate and the counterpart. Thus direct tribological contact of the two surfaces with a subsequent oxide formation occurs and lubrication vanishes.

3.3.2 1 µm/CNT sample

The evaluation of the wear track of the **1 µm/CNT** sample after **18000 cycles** is illustrated in **Fig. 7a**.

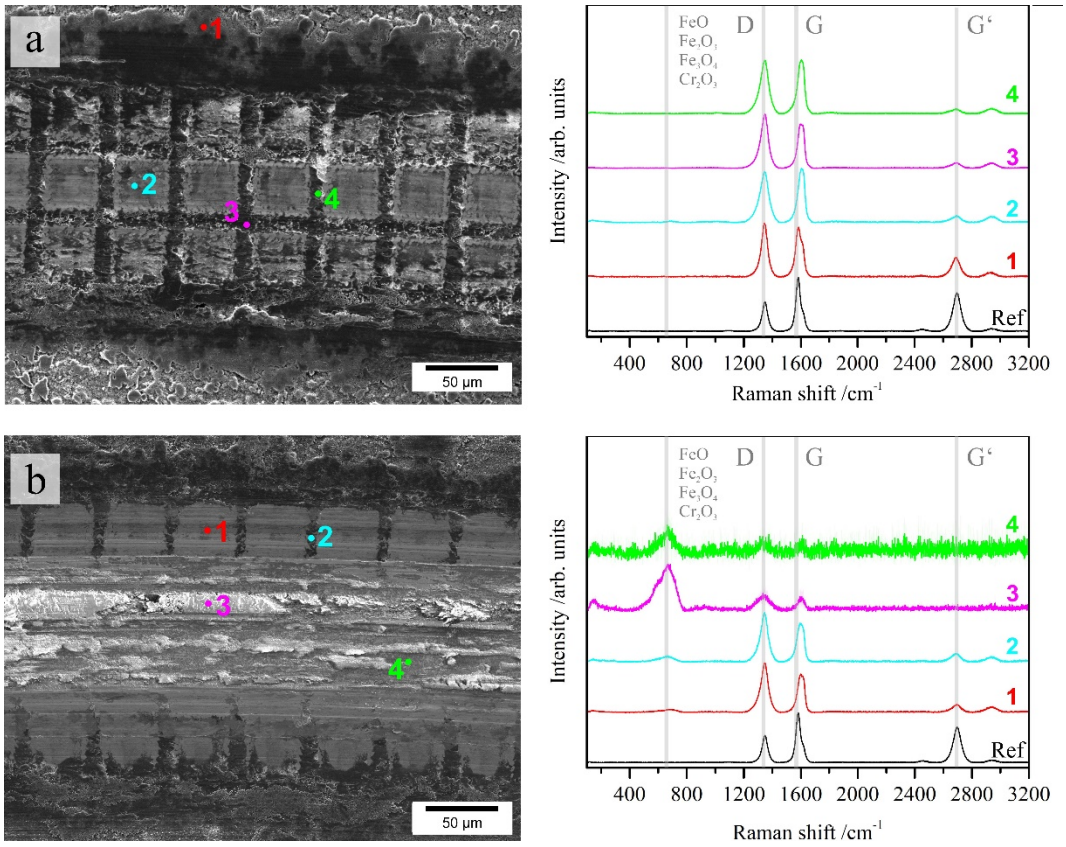

Figure 7 – 1 µm/CNT sample after (a) 18000 cycles and (b) after reaching the reference steady state friction coefficient (110000 cycles).

Contrary to what would be expected after a significant amount of cycles, no oxides can be detected in the entirety of the wear track. Even in the center of the track, CNTs can be detected in both, the topography maximum (2) and minimum (3, 4) of the laser structures. Accordingly and as the surfaces were already slightly oxidized in their initial state due to laser structuring, the acquisition depth of the Raman characterization can also be listed as a possible cause for the absence of oxidic resonances. However, a closer examination of the characteris-

tic CNT peak positions and their intensity ratios (as listed in **Table 2**) in the spectra from the center of the wear track (2 - 4) reveals a structural degradation of the CNTs - similar to that on the **Ref/CNT sample**. The defect index has similarly high values (≥ 1) as **Ref/CNT**. The G-band upshift (approximately 1600 cm^{-1}) also indicates a structural state similar to nanocrystalline graphite.

Table 2 – Structural assessment of the CNTs at different stages of the tribological test.

After 18000 cycles					**After reaching steady state reference COF**				
Sample		**I_D/I_G**	**X_{CG}**		**Sample**		**I_D/I_G**	**X_{CG}**	
	Ref	0.55	1582.1			Ref	0.55	1582.1	
1 µm /CNT	1	1.08	1583.1		1 µm /CNT (110k cycles)	1	1.30	1599.5	
	2	0.93	1605.9			2	1.29	1595.1	
	3	1.23	1600.5			3	1.23	1591.9	
	4	0.99	1603.8			4	1.04	1600.8	

Yet, **after 18000 cycles,** the friction curves of this sample show a stable low COF (0.14) in the equilibrium state. Accordingly, the structural integrity of the CNTs seems to play only a minor role in maintaining the lubricating effect. Rather, the presence of a sufficient quantity of MWCNT in tribological contact and its continuous transport from the laser-induced lubricant reservoirs to the contact seems to be the dominant effect. In addition, the lubrication mechanism in the area of damaged CNTs can be based on their rolling/sliding ability on the one hand, but also on the lubricating behavior of graphite on the other hand.

The corresponding Raman evaluation of the sample type **1µm/CNT after reaching steady state reference COF (110000 cycles)** is shown in **Fig. 7b**. As already discussed before, only small amounts of oxidic substances are detected in the outer area of the wear track (measurement points 1 and 2). Based on the intensity ratios listed in **Table 2**, it is clear that the defect density of the MWCNTs in these ranges is higher than in the CNT initial state. In addition, the G-peak positions of the CNTs at both, the topography maxima and minima are again upshifted to 1599.5 cm^{-1} and 1595.1 cm^{-1}, respectively, indicating a structural degradation [49]. However, it should be noted that the detected peaks result from an averaging of all radiated CNTs. This means that in the minima, completely unaffected CNTs can still be stored, which to the moment have not had to bear any mechanical load. In the center of the wear track (**Fig. 7b point 3**), on the other hand, the intensity of the oxide peak at 670 cm^{-1} increases and that of the CNT peaks decrease significantly. The G'-band is no longer detected.

As already mentioned, the absence of the protective CNT layer leads to a tribochemical oxidation and the generation of third bodies, which results in the observed steep rise in COF. At the bright spots in the center of the track (4), the low intensity values are overlaid by a noisy signal typical for pure metallic substances. The presence of oxides and the characteristic CNT bands at these sites is due to the comparatively large laser spot size of the Raman microscope (approximately 5 µm).

3.3.3 3 µm/CNT sample

For the sample **3 µm/CNT after 18000 cycles**, the evaluated Raman spectra evidences CNTs everywhere in the wear track area (**Fig. 8a**), whereby a low intensity oxide peak can be detected in the region of the laser-induced structure minimum (4).

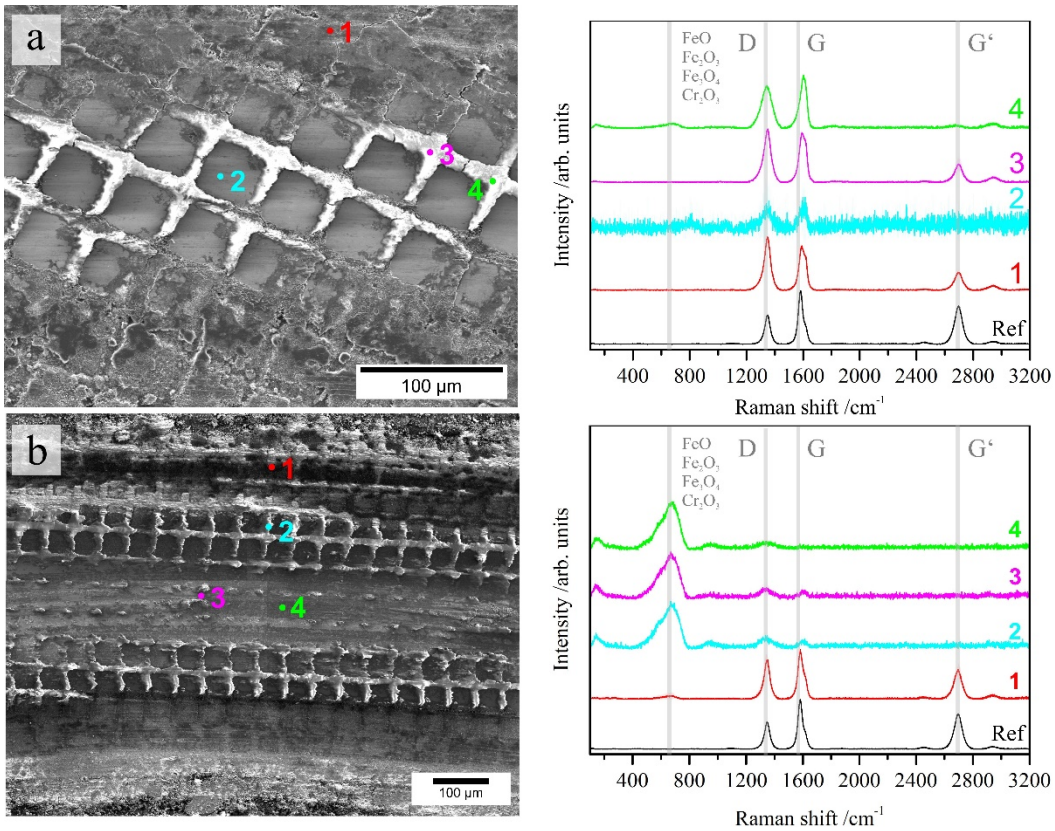

Figure 8 – 3 µm/CNT sample after (a) 18000 cycles and (b) after reaching the reference steady state friction coefficient (57000 cycles).

This is correlated with initially present surface oxidation due to the laser process and wear particles generated by previous abrasion of the initial, oxidized material pilings. These particles can be transported by the sphere into the minima positions of the surface structure, as

discussed in [45]. Furthermore, the Raman spectrum at position 2 indicates that only small signals of the CNT bands are still acquired on the substrate within the wear track (**Figure 8a**). In combination with the observed signal noise, it can be confirmed that in this sample type there is direct contact between the surfaces of the contact partners after only 18000 cycles, which leads to an increase in friction and wear. The increase in COF (0.43), which has already occurred, confirms this observation. As with the other two coated samples, damage to the CNTs is observed to have already occurred on the basis of the values listed in **Table 3**.

Table 3 – Structural assessment of the CNTs at different stages of the tribological test.

After 18000 cycles					**After reaching steady state reference COF**				
Sample		**I_D/I_G**	**X_{CG}**		**Sample**		**I_D/I_G**	**X_{CG}**	
	Ref	0.55	1582.1			Ref	0.55	1582.1	
3 µm /CNT	1	1.22	1590.7		3 µm /CNT (57k cycles)	1	0.79	1582.1	
	2	0.91	1613.5			2	1.31	1604.2	
	3	1.08	1592.9			3	1.20	1606.5	
	4	0.80	1602.7			4	--	--	

The lack of lubricant in contact and the inadequate continuous feed into contact are the main factors affecting the lubrication process. Although small amounts of CNTs can be brought into contact, this is not enough to effectively separate the contacting surfaces from each other and hence, contribute to a continuous reduction of friction.

The Raman spectra of the characteristic areas of the wear track **after reaching the steady state COF of the reference at 57000 cycles** are shown in **Fig. 8b**. Barely modified CNTs which were pulled out of the contact are observed only in the outer area (1) with only a small oxide peak at 670 cm^{-1} (see also **Table 3**). In contrast to the sample **1 µm/CNT**, even the laser-induced minima in the outer area of the track show a pronounced oxide peak and a G-peak shifted to 1604.2 cm^{-1}. According to [49], such a wide upshifting of the G-peak beyond a wavenumber of 1600 cm^{-1} is not expected. This can be justified by the spectral resolution of the Raman microscope used (1.2 cm^{-1}) in combination with inaccuracies with the profile (Lorentz) fitting. Along with an increased defect density of 1.31 and the absence of the G' peak, it can be assumed that the CNTs are indeed degraded and again, transitioned into nanocrystalline graphite. At the same time, the largest shift of the G-peak (1606.5 cm^{-1}) can be seen there, whereas in the measuring range of point 4, this is no longer observed at all.

These findings confirm the assumptions made that there are no more noticeable amounts of CNTs in the entire wear track and that they disappear as the test evolves.

4. Conclusions

In the present study, a systematic evaluation of the influence of surface structure design on the solid lubrication effect of multi-walled carbon nanotubes (MWCNT) coated steel surfaces is provided. An efficient lubrication is achieved for all MWCNT coated surfaces with a maximum 6-fold frictional reduction compared to the steel reference and friction coefficients as low as 0.14. In case of the cross-like surface pattern with a structural depth of 1 µm, a 9-fold extension of the lubrication lifetime compared to the MWCNT coated, unstructured sample is observed. However, and in contrast to what would be expected, it is shown that deeper structures (3 µm structural depth) with larger lubricant storage volume do not lead to an extended lubrication lifetime and behave almost equally to the coated unstructured surfaces. This can be attributed, among other things, to the formation of high profile deposits at the edges of the surface depressions due to displaced molten material and material redepositioning as well as a higher slope steepness of the structures, which prevent efficient lubricant supply into the contact. The lubrication of MWCNT coatings is found to be based on the high aspect ratio of MWCNT allowing them to be dragged into the tribological contact as well as an elastic restoration of the coating after compaction during the tribological contact. The lubrication mechanism of the CNT is a mixture between graphite lubrication and their ability to perform complex motions and act as separating layer between the contacting surfaces. This study highlights the importance of a carefully selected surface design in order to achieve beneficial effects with regard to MWCNTs as solid lubricant coatings.

Acknowledgements

The present work is supported by funding from the Deutsche Forschungsgemeinschaft (DFG, project: MU 959/38-1 and SU 911/1-1). The authors wish to acknowledge the EFRE Funds of the European Commission for support of activities within the AME-Lab project. This work was supported by the CREATe-Network Project, Horizon 2020 of the European Commission (RISE Project No. 644013). We thank Prof. Volker Presser (INM, Saarbrücken) for providing access to the Raman spectrometer and SFB 926 ”Microscale Morphology of Component Surfaces” CRC 926 for measurements by Auger electron spectroscopy.

References

[1] Etsion I. State of the Art in Laser Surface Texturing. J Tribol 2005;127:248. doi:10.1115/1.1828070.

[2] Gachot C, Rosenkranz A, Reinert L, Ramos-Moore E, Souza N, Müser MH, et al. Dry friction between laser-patterned surfaces: Role of alignment, structural wavelength and surface chemistry. Tribol Lett 2013;49:193–202. doi:10.1007/s11249-012-0057-y.

[3] Rosenkranz A, Reinert L, Gachot C, Mücklich F. Alignment and wear debris effects between laser-patterned steel surfaces under dry sliding conditions. Wear 2014;318:49–61. doi:10.1016/j.wear.2014.06.016.

[4] Szurdak A, Rosenkranz A, Gachot C, Hirt G, Mücklich F. Manufacturing and Tribological Investigation of Hot Micro-Coined Lubrication Pockets. Key Eng Mater 2014;611–612:417–24. doi:10.4028/www.scientific.net/KEM.611-612.417.

[5] Koszela W, Pawlus P, Galda L. The effect of oil pockets size and distribution on wear in lubricated sliding. Wear 2007;263:1585–92. doi:10.1016/j.wear.2007.01.108.

[6] Pettersson U, Jacobson S. Influence of surface texture on boundary lubricated sliding contacts. Tribol Int 2003;36:857–64. doi:10.1016/S0301-679X(03)00104-X.

[7] Pawlus P. Effects of honed cylinder surface topography on the wear of piston-piston ring-cylinder assemblies under artificially increased dustiness conditions. Tribol Int 1993;26:49–55. doi:10.1016/0301-679X(93)90038-3.

[8] Lasagni A, Roch T, Bieda M, Benke D, Beyer E. High speed surface functionalization using direct laser interference patterning, towards 1 m 2 /min fabrication speed with sub-µm resolution. Proc SPIE 2014;8968:89680A. doi:10.1117/12.2041215.

[9] Mücklich F, Lasagni A, Daniel C. Laser Interference Metallurgy – using interference as a tool for micro/nano structuring. Zeitschrift Für Met 2006;97:1337–44.

[10] Rosenkranz A, Heib T, Gachot C, Mücklich F. Oil film lifetime and wear particle analysis of laser-patterned stainless steel surfaces. Wear 2015;334–335:1–12. doi:10.1016/j.wear.2015.04.006.

[11] Rosenkranz A, Krupp F, Reinert L, Mücklich F, Sauer B. Tribological performance of laser-patterned chain links – Influence of pattern geometry and periodicity. Wear 2017;370–371:51–8. doi:10.1016/j.wear.2016.11.006.

[12] Grützmacher PG, Rosenkranz A, Gachot C. How to guide lubricants - Tailored laser surface patterns on stainless steel. Appl Surf Sci 2016;370:59–66. doi:10.1016/j.apsusc.2016.02.115.

[13] Rapoport L, Moshkovich A, Perfilyev V, Lapsker I, Halperin G, Itovich Y, et al. Friction and wear of MoS2 films on laser textured steel surfaces. Surf Coatings Technol 2008;202:3332–40.

[14] Cho MH, Ju J, Kim SJ, Jang H. Tribological properties of solid lubricants (graphite, Sb2S3, MoS2) for automotive brake friction materials. Wear 2006;260:855–60. doi:10.1016/j.wear.2005.04.003.

[15] Scharf TW, Prasad S V. Solid lubricants: A review. J Mater Sci 2013;48:511–31. doi:10.1007/s10853-012-7038-2.

[16] Zhai W, Srikanth N, Kong LB, Zhou K. Carbon nanomaterials in tribology. Carbon N Y 2017;119:150–71. doi:10.1016/j.carbon.2017.04.027.

[17] Chen W, Tu J, Wang L, Gan H, Xu Z. Tribological application of carbon nanotubes in a metal-based composite coating and composites. Carbon N Y 2003;41:215–22.

[18] Kim KT, Cha S Il, Hong SH. Hardness and wear resistance of carbon nanotube reinforced Cu matrix nanocomposites. Mater Sci Eng A 2007;449–451:46–50. doi:10.1016/j.msea.2006.02.310.

[19] Scharf T, Neira A, Hwang JY, Tiley J, Banerjee R. Self-lubricating carbon nanotube reinforced nickel matrix composites. J Appl Phys 2009;106:13508. doi:10.1063/1.3158360.

[20] Tan J, Yu T, Xu B, Yao Q. Microstructure and wear resistance of nickel–carbon nanotube composite coating from brush plating technique. Tribol Lett 2006;21:107–11. doi:10.1007/s11249-006-9025-8.

[21] Suárez S, Rosenkranz A, Gachot C, Mücklich F. Enhanced tribological properties of MWCNT/Ni bulk composites - Influence of processing on friction and wear behaviour. Carbon N Y 2014;66:164–71. doi:10.1016/j.carbon.2013.08.054.

[22] Reinert L, Suárez S, Rosenkranz A. Tribo-Mechanisms of Carbon Nanotubes : Friction and Wear Behavior of CNT-Reinforced Nickel Matrix Composites and CNT-Coated Bulk Nickel. Lubricants 2016;4:1–15. doi:10.3390/lubricants4020011.

[23] Miyoshi K, Street KW, Vander Wal RL, Andrews R, Sayir A. Solid lubrication by multiwalled carbon nanotubes in air and in vacuum. Tribol Lett 2005;19:191–201. doi:10.1007/s11249-005-6146-4.

[24] Hirata A, Yoshioka N. Sliding friction properties of carbon nanotube coatings deposited by microwave plasma chemical vapor deposition. Tribol Int 2004;37:893–8.

[25] Hu JJ, Jo SH, Ren ZF, Voevodin a. a., Zabinski JS. Tribological behavior and graphitization of carbon nanotubes grown on 440C stainless steel. Tribol Lett 2005;19:119–25. doi:10.1007/s11249-005-5091-6.

[26] Dickrell PL, Pal SK, Bourne GR, Muratore C, Voevodin AA, Ajayan PM, et al. Tunable friction behavior of oriented carbon nanotube films. Tribol Lett 2006;24:85–90. doi:10.1007/s11249-006-9162-0.

[27] Reinert L, Schütz S, Suárez S, Mücklich F. Influence of Surface Roughness on the Lubrication Effect of Carbon Nanoparticle-Coated Steel Surfaces. Tribol Lett 2018;66:45. doi:10.1007/s11249-018-1001-6.

[28] Chen CS, Chen XH, Xu LS, Yang Z, Li WH. Modification of multi-walled carbon nanotubes with fatty acid and their tribological properties as lubricant additive. Carbon N Y 2005;43:1660–6. doi:10.1016/j.carbon.2005.01.044.

[29] Peng Y, Hu Y, Wang H. Tribological behaviors of surfactant-functionalized carbon nanotubes as lubricant additive in water. Tribol Lett 2007;25:247–53. doi:10.1007/s11249-006-9176-7.

[30] Lu HF, Fei B, Xin JH, Wang RH, Li L, Guan WC. Synthesis and lubricating performance of a carbon nanotube seeded miniemulsion. Carbon N Y 2007;45:936–42. doi:10.1016/j.carbon.2007.01.001.

[31] Kristiansen K, Zeng H, Wang P, Israelachvili JN. Microtribology of aqueous carbon nanotube dispersions. Adv Funct Mater 2011;21:4555–64. doi:10.1002/adfm.201101478.

[32] Falvo MR, Taylor RM, Helser A, Chi V, Brooks FP, Washburn S, et al. Nanometre-scale rolling and sliding of carbon nanotubes. Nature 1999;397:236–8. doi:10.1038/16662.

[33] Chen XH, Chen CS, Xiao HN, Liu HB, Zhou LP, Li SL, et al. Dry friction and wear characteristics of nickel/carbon nanotube electroless composite deposits. Tribol Int 2006;39:22–8. doi:10.1016/j.triboint.2004.11.008.

[34] Dickrell PL, Sinnott SB, Hahn DW, Raravikar NR, Schadler LS, Ajayan PM, et al. Frictional anisotropy of oriented carbon nanotube surfaces. Tribol Lett 2005;18:59–62.

[35] Majumder M, Rendall C, Li M, Behabtu N, Eukel JA, Hauge RH, et al. Insights into the physics of spray coating of SWNT films. Chem Eng Sci 2010;65:2000–8. doi:10.1016/j.ces.2009.11.042.

[36] Mirri F, Ma AWK, Hsu TT, Behabtu N, Eichmann SL, Young CC, et al. High-performance carbon nanotube transparent conductive films by scalable dip coating. ACS Nano 2012;6:9737–44. doi:10.1021/nn303201g.

[37] Bardecker JA, Afzali A, Tulevski GS, Graham T, Hannon JB, Jen AKY. Directed assembly of single-walled carbon nanotubes via drop-casting onto a UV-patterned photosensitive monolayer. J Am Chem Soc 2008;130:7226–7. doi:10.1021/ja802407f.

[38] De Nicola F, Castrucci P, Scarselli M, Nanni F, Cacciotti I, De Crescenzi M. Super-hydrophobic multi-walled carbon nanotube coatings for stainless steel. Nanotechnology 2015;26:145701. doi:10.1088/0957-4484/26/14/145701.

[39] Boccaccini AR, Cho J, Roether J a., Thomas BJC, Jane Minay E, Shaffer MSP. Electrophoretic deposition of carbon nanotubes. Carbon N Y 2006;44:3149–60. doi:10.1016/j.carbon.2006.06.021.

[40] Thomas BJC, Boccaccini AR, Shaffer MSP. Multi-Walled Carbon Nanotube Coatings Using Electrophoretic Deposition (EPD). J Am Ceram Soc 2005;88:980–2.

[41] Cho J, Konopka K, Rozniatowski K, Garcia-Lecina E, Shaffer MSP, Boccaccini AR. Characterisation of carbon nanotube films deposited by electrophoretic deposition. Carbon N Y 2009;47:58–67. doi:10.1016/j.carbon.2008.08.028.

[42] Van der Biest OO, Vandeperre LJ. Electrophoretic deposition of materials. Annu Rev Mater Sci 1999;29:327–52. doi:10.1146/annurev.matsci.29.1.327.

[43] Sarkar P, Nicholson PS. Electrophoretic deposition (EPD): Mechanisms, kinetics, and application to ceramics. J Am Ceram Soc 1996;79:1987–2002. doi:10.1111/j.1151-2916.1996.tb08929.x.

[44] Boccaccini AR, Zhitomirsky I. Application of electrophoretic and electrolytic deposition techniques in ceramics processing. Curr Opin Solid State Mater Sci 2002;6:251–60.

[45] Reinert L, Lasserre F, Gachot C, Grützmacher P, MacLucas T, Souza N, et al. Long-lasting solid lubrication by CNT-coated patterned surfaces. Sci Rep 2017;7:42873. doi:10.1038/srep42873.

[46] Lasagni A. Advanced design of periodical structures by laser interference metallurgy in the micro / nano scale on macroscopic areas. Saarland University, 2006.

[47] Lasagni A, D'Alessandria M, Giovanelli R, Mücklich F. Advanced design of periodical architectures in bulk metals by means of Laser Interference Metallurgy. Appl Surf Sci 2007;254:930–6. doi:10.1016/j.apsusc.2007.08.010.

[48] Leitz K-H, Redlingshöfer B, Reg Y, Otto A, Schmidt M. Metal Ablation with Short and Ultrashort Laser Pulses. Phys Procedia 2011;12:230–8. doi:10.1016/j.phpro.2011.03.128.

[49] Ferrari A, Robertson J. Interpretation of Raman spectra of disordered and amorphous carbon. Phys Rev B 2000;61:14095–107. doi:10.1103/PhysRevB.61.14095.

[50] Thomas BJC, Shaffer MSP, Freeman S, Koopman M, Chawla KK, Boccaccini AR. Electrophoretic Deposition of Carbon Nanotubes on Metallic Surfaces. Key Eng Mater 2006;314:141–6. doi:10.4028/www.scientific.net/KEM.314.141.

[51] Le Harzic R, Breitling D, Weikert M, Sommer S, Föhl C, Dausinger F, et al. Ablation comparison with low and high energy densities for Cu and Al with ultra-short laser pulses. Appl Phys A 2005;80:1589–93. doi:10.1007/s00339-005-3206-4.

[52] Johnson KL. Contact Mechanics. 1st ed. New York, NY, USA: Cambridge University Press; 1985.

[53] Bonse J, Krüger J, Höhm S, Rosenfeld A. Femtosecond laser-induced periodic surface structures. J Laser Appl 2012;24:42006. doi:10.2351/1.4712658.

[54] Raillard B, Gouton L, Ramos-Moore E, Grandthyll S, Müller F, Mücklich F. Ablation effects of femtosecond laser functionalization on steel surfaces. Surf Coatings Technol 2012;207:102–9. doi:10.1016/j.surfcoat.2012.06.023.

[55] Lehman JH, Terrones M, Mansfield E, Hurst KE, Meunier V. Evaluating the characteristics of multiwall carbon nanotubes. Carbon N Y 2011;49:2581–602. doi:10.1016/j.carbon.2011.03.028.

[56] DiLeo RA, Landi BJ, Raffaelle RP. Purity assessment of multiwalled carbon nanotubes by Raman spectroscopy. J Appl Phys 2007;101. doi:10.1063/1.2712152.

[57] Shimada T, Sugai T, Fantini C, Souza M, Cançado LG, Jorio A, et al. Origin of the 2450 cm-1 Raman bands in HOPG, single-wall and double-wall carbon nanotubes. Carbon N Y 2005;43:1049–54. doi:10.1016/j.carbon.2004.11.044.

[58] Dresselhaus MS, Dresselhaus G, Saito R, Jorio a. Raman spectroscopy of carbon nanotubes. Phys Rep 2005;409:47–99. doi:10.1016/j.physrep.2004.10.006.

[59] Oh SJ, Cook DC, Townsend HE. Characterization of iron oxides commonly formed as corrosion products on steel. Hyperfine Interact 1998;112:59–66.

[60] McCarty KF, Boehme DR. A Raman study of the systems Fe3−xCrxO4 and Fe2−xCrxO3. J Solid State Chem 1989;79:19–27. doi:10.1016/0022-4596(89)90245-4.

[61] Farrow R., Benner R., Nagelberg A., Mattern P. Characterization of surface oxides by Raman spectroscopy. Thin Solid Films 1980;73:353–8. doi:10.1016/0040-6090(80)90499-X.